RSC Advances

PAPER

Check for updates

Multidimensional insights involving electrochemical and *in silico* investigation into the corrosion inhibition of newly synthesized pyrazolotriazole derivatives on carbon steel in a HCl solution†

Lei Guo, [ID] *[a] Youness El Bakri,*[bc] El Hassane Anouar, [ID] *[d] Jianhong Tan,[e] Savaş Kaya[f] and El Mokhtar Essassi[b]

Herein, the anti-corrosion of carbon steel in 1 M HCl by two newly synthesized pyrazolotriazole derivatives, namely, 6-methyl-1*H*-pyrazolo[5,1-*c*][1,2,4]triazole-7-carbonitrile (CPT) and 1-acetyl-6-methyl-1*H*-pyrazolo[5,1-*c*][1,2,4]triazole-7-carbothioamide (MPT), was studied using electrochemical, density functional theory (DFT), and molecular dynamics (MD) simulation techniques. The experimental results showed that the concentrations of inhibitors had a significant influence on their inhibition efficiencies. Potentiodynamic polarization curves indicated that the two pyrazolotriazoles were mixed-type inhibitors. DFT calculations were employed to explore the molecular activity, and MD simulations were performed to obtain the interaction energy between the inhibitor molecules and the iron surface. The findings obtained using the theoretical calculation techniques were consistent with those obtained *via* experiments.

1. Introduction

Nowadays, hydrochloric acid solutions are being widely applied in industrial fields such as acid pickling, industrial cleaning, acid descaling, oil-well acidizing and petrochemical processes. In these applications, the service metals (usually carbon steel) can be subjected to different degrees of processing;[1] in this regard, the use of an organic corrosion inhibitor is the most important and economical approach among all anticorrosive methods.[2–4] Majority of researchers believe that inhibitors protect metals from corrosion by forming a film on the metal substrate.[5–7] Their inhibition effectiveness is generally related to

[a]School of Material and Chemical Engineering, Tongren University, Tongren 554300, China. E-mail: cqglei@163.Icom

[b]Laboratoire de Chimie Organique Hétérocyclique, Centre de Recherche des Sciences des Médicaments, Pôle de Compétences Pharmacochimie, URAC 21, Faculté des Sciences, Mohammed V University Rabat, Avenue Ibn Battouta, BP 1014, Rabat, Morocco. E-mail: yns.elbakri@gmail.com

[c]Organic Chemistry Department, Science Faculty, RUDN University, Miklukho-Maklaya St. 6, Moscow 117198, Russian Federation

[d]Department of Chemistry, College of Science and Humanities, Prince Sattam Bin Abdulaziz University, P. O. Box 83, Al Kharj 11942, Saudi Arabia. E-mail: anouarelhassane@yahoo.fr

[e]School of Chemistry and Chemical Engineering, Yangtze Normal University, Chongqing 408100, China

[f]Cumhuriyet University, Faculty of Science, Department of Chemistry, Sivas 58140, Turkey

† Electronic supplementary information (ESI) available. See DOI: 10.1039/c9ra05881h

their chemical composition, molecular volume, water solubility, heat stability, and affinity to the metal substrate.[8] Polar functional groups, heteroatoms, such as O, N, S, and P atoms, and π-electrons act as adsorption centers during metal–inhibitor interactions. We have theoretically confirmed an empirical rule that the general trend of the inhibition efficiencies of molecules containing heteroatoms is O < N < S.[9]

As is well-known, the corrosion inhibition properties of organic molecules depend on their molecular activity. These molecular descriptors can be obtained from quantum chemical approaches, which have been widely used to explore the reaction mechanism.[10,11] Generally, the design and application of inhibitors with larger molecular sizes is an effective strategy to ensure their corrosion inhibition efficiency, which may provide a better surface coverage.[12] Some researchers have studied the inhibition mechanism of organic inhibitors through DFT calculations, and some linear or nonlinear models based on multiple regressions have been successfully established to probe the relationship between quantum chemical descriptors and inhibition efficiency.[13–15] On the other hand, molecular dynamics simulation is a valid approach to obtain information about the interaction between the metal substrate and inhibitor molecules.[16] Pyrazolotriazole is a heterocyclic aromatic organic compound with a bicyclic structure consisting of fused pyrazole and triazole rings. Some studies have demonstrated that pyrazolotriazole derivatives are safe and nontoxic to humans or the environment, and thus, they can be used as antimicrobial agents or PDE4 inhibitors.[17,18] In addition, many researches

have indicated that triazole derivatives can serve as excellent inhibitors for metal corrosion in an acidic medium.[19-21] Thus, pyrazolotriazoles with large volumes can be theoretically used in metal corrosion and protection applications.

The purpose of this study was to investigate the inhibition effect of two newly synthesized pyrazolotriazoles on the corrosion of carbon steel in a molar hydrochloric acid solution. Electrochemical tests were carried out, and the anticorrosive mechanism was clarified. Moreover, the effects of temperature and inhibitor concentration on the inhibition performance were investigated. In addition, detailed DFT calculations and MD simulations were conducted to corroborate the experimental observation. The results presented in this study would benefit the development of novel inhibitors with a better efficacy for carbon steel in an acid solution through rational molecular preconstruction.

2. Materials and methods

2.1. Synthesis of pyrazolotriazole derivatives

Typically, 1 g of 6-methyl-7H-[1,2,4]triazolo[4,3-b][1,2,4]triazepine-8(9H)-thione was heated in 10 ml acetic anhydride for 1 h. The solution was then concentrated to dryness under reduced pressure, and the residue obtained was extracted with dichloromethane. After concentrating the solution under vacuum, the obtained solid was subjected to chromatography using a silica column (eluent: dichloromethane/methanol: 95/5 v/v). We separated the two products MPT and CPT, and their relevant structural information is presented in Table 1 and Fig. S1–S4 (ESI†).

MPT. Off-white solid, yield: 18%; mp: 202–204 °C. ^{1}H NMR (300 MHz, DMSO) δ ppm: 9.34 (s, 1H, CH$_{triazolic}$); 2.59 (s, 3H, CH$_3$); 2.40 (s, 3H, CH$_3$). ^{13}C NMR (75 MHz, DMSO) δ ppm: 167.77, 161.78, 143.57, 113.44, 73.40 (Cq); 133.23 (CH) 21.23, 13.92 (CH$_3$). Elemental analysis: calculated: C, 43.04%; H, 4.06%; N, 31.37%; O, 7.17%; and S, 14.36%. Found: C, 43.13%; H, 4.01%; N, 31.29%; O, 7.18%; and S, 14.39%.

CPT. White solid, yield: 20%; mp: 188–190 °C. ^{1}H NMR (300 MHz, DMSO) δ 9.06 (s, 1H, CH$_{triazolic}$); 2.34 (s, 3H, CH$_3$)·^{13}C NMR (75 MHz, DMSO) δ ppm: 160.91, 147.43, 114.84, 64.48 (Cq); 130.78 (CH); 13.98 (CH$_3$). Elemental analysis: calculated: C, 48.98%; H, 3.43%; and N, 47.60%. Found: C, 48.97%; H, 3.44%; and N, 47.59%.

To validate that the synthesized inhibitors were environmentally non-toxic, the toxicities of CPT and MPT were evaluated using the TOPKAT module of the Discovery studio 3.0 software.[22] The obtained probability values indicated that the toxic levels of both inhibitors were in a safe area (see ESI† for more details on the toxicity data).
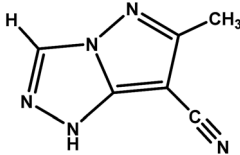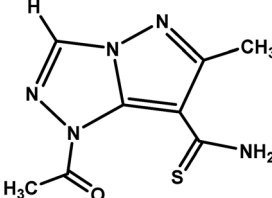
2.2. Preparation of test solutions and electrodes

The corrosion tests were performed in a 1 M HCl solution in the absence and presence of pyrazolotriazole derivatives at various concentrations ranging from 10^{-6} M to 10^{-3} M. The corrosive solution was prepared by diluting HCl (analytical grade 37%) with distilled water. Carbon steel was used, which was subjected to metallographic preparation with the following nominal composition: 0.36 wt% C, 0.66 wt% Mn, 0.27 wt% Si, 0.02 wt% S, 0.015 wt% P, 0.21 wt% Cr, 0.02 wt% Mo, 0.22 wt% Cu, 0.06 wt% Al and the rest iron. Before each experiment, the electrodes were successively abraded with sand papers of different grades followed by washing with ethanol and distilled water. The effect of temperature on the inhibition efficiencies of the inhibitors was tested between 303 and 333 K.

2.3. Electrochemical measurements

Electrochemical impedance spectroscopy (EIS) and potentiodynamic polarization (PDP) measurements were carried out using an EG&G Princeton Applied Research Parc Model 2273. A three-electrode electrolytic cell was employed with carbon steel as the working electrode, platinum foil as the counter electrode, and saturated calomel as the reference electrode. The tested area of the electrodes exposed to the solution was 1 cm^2. The

Table 1 Some information about the newly synthesized pyrazolotriazole derivatives

Inhibitor	Structure	Abbreviation	Molar mass (g mol^{-1})
6-Methyl-1H-pyrazolo[5,1-c][1,2,4]triazole-7-carbonitrile		CPT	147.14
1-Acetyl-6-methyl-1H-pyrazolo[5,1-c][1,2,4]triazole-7-carbothioamide		MPT	223.25

carbon steel electrode was immersed in the corrosive solution for an appropriate time until a steady-state potential was achieved. EIS measurements were performed by applying a 10 mV sine wave with frequencies in the range of 100 kHz to 10 mHz to the cell. The polarization curves were obtained by polarization at the scan rate of 0.167 mV s^{-1}. The data obtained by the PDP methods were analyzed and fitted using the Ec-Lab analysis software, and the impedance results were fitted using the Zview impedance analysis software.

2.4. DFT calculations

Initially, the ground states of the synthesized pyrazolotriazoles derivatives were optimized using the state-of-art DFT method, for which the famous hybrid functional B3LYP was used *via* the Dmol^3 code in the Materials Studio software.[23] The minima of the optimized structures of the tilted compounds were confirmed by frequency calculations at the same level of theory (*i.e.*, the absence of imaginary frequencies). The effects of the solvent molecules were implicitly taken into account by considering the conductor-like screening model.[24] In the defined model, the solute was embedded into a cavity surrounded by solvent molecules, which were described by the dielectric constant ε (*e.g.*, for water, $\varepsilon = 78.3$). Then, the relevant quantum chemical parameters were obtained.

2.5. Molecular dynamics simulation

An MD simulation was conducted using the Forcite module of the Materials Studio 8.0 program developed by BIOVIA Inc. The simulation was carried out in a simulation box (1.98 nm × 1.98 nm × 4.81 nm) with periodic boundary conditions to model a representative part of the interface devoid of any arbitrary boundary effects. The box consisted of an iron slab and a water slab (with 500 water molecules) containing the studied inhibitor. For the iron surface, an Fe(110) surface has been selected as the studied surface because Fe(110) has a density packed surface and is most stable.[25] The Fe(110) surface was modeled with a six-layer slab model. In this model, there were 64 iron atoms in each layer representing an (8 × 8) unit cell. The entire system was performed at 303 K, controlled by an Andersen thermostat, NVT ensemble, with a time step of 1.0 fs and a simulation time of 1000 ps using the COMPASS force field.[26] Non-bonding interactions, *i.e.* van der Waals and electrostatic interactions, were set for the atom-based and Ewald summation method, respectively, with the cut off radius of 1.55 nm.

3. Results and discussion

3.1. PDP measurements

Potentiodynamic polarization curves for carbon steel in a 1 M HCl solution without and with pyrazolotriazoles at different concentrations at 303 K are presented in Fig. 1. As observed from Fig. 1, the nature of the polarization curves did not change with and without inhibitors; however, the curves shifted towards lower current density after the addition of inhibitors; this suggested that the inhibitor molecules inhibited the

corrosion process. The values of corrosion current densities (I_{corr}) were determined by the extrapolation of the cathodic and anodic Tafel lines to the corrosion potential (E_{corr}). The electrochemical parameters, including the E_{corr}, I_{corr}, anodic Tafel slope (β_a), cathodic Tafel slope (β_c), and percentage inhibition efficiency (IE%), are presented in Table 2. The inhibition efficiencies were evaluated using the following equation:

$$IE(\%) = \frac{I_{corr,0} - I_{corr}}{I_{corr,0}} \times 100 \qquad (1)$$

where I_{corr} and $I_{corr,0}$ denote the corrosion current densities with and without inhibitors, respectively.

The results presented in Table 2 revealed that an increase in the concentration of both derivatives resulted in a decrease in the corrosion current densities and an increase in the inhibition efficiency, suggesting that the adsorption of the inhibitor molecules on the surface of carbon steel blocked the active sites. Particularly, it is worth mentioning that the optimal inhibition efficiencies for the two compounds follow the order CPT < MPT, and the values are 89.6% and 93.5%, respectively. The presence of inhibitors caused a minor change in the E_{corr} values (less than 85 mV) with respect to the case of the blank; this implied that both organics acted as mixed-type inhibitors.[27] They not only would reduce the anodic dissolution of carbon steel, but would also retard the cathodic hydrogen evolution reaction. Moreover, it was obvious that the slopes of the anodic (β_a) and cathodic (β_c) Tafel lines remained almost unchanged upon the addition of the two compounds. This indicated that the inhibitors decreased the surface area for corrosion without affecting the corrosion mechanism of carbon steel in the HCl solutions.[28] The inhibiting effect of the inhibitors may be related to their adsorption and the formation of a barrier film on the electrode surface.

3.2. EIS measurements

The EIS measurements were carried out to further evaluate the corrosion inhibition performance of these two new inhibitors. The impedance spectra for carbon steel in 1.0 M HCl with and without CPT and MPT at different concentrations at 303 K are presented as Nyquist plots in Fig. 2. The plots are denoted by a unitary capacitive loop in the form of depressed semicircles. A deviation of this kind is often referred to as frequency dispersion due to the surface inhomogeneity of the working electrode.[29] It is clear from Fig. 2 that the impedance response of carbon steel has significantly changed after the addition of pyrazolotriazoles to the corrosive solution. The diameters of the capacitive loops increased with an increase in the inhibitor concentration. Generally, a large charge transfer resistance is associated with a slowly corroding system. It was worth noting that the change in the concentrations of inhibitors did not alter the shape of the impedance behavior; this implied a similar inhibition mechanism of the inhibitors.

Fig. 3 shows the equivalent circuit model for the analysis of the impedance characteristics. Herein, R_s represents the solution resistance and R_{ct} is the charge transfer resistance corresponding to the corrosion reaction at the iron–solution
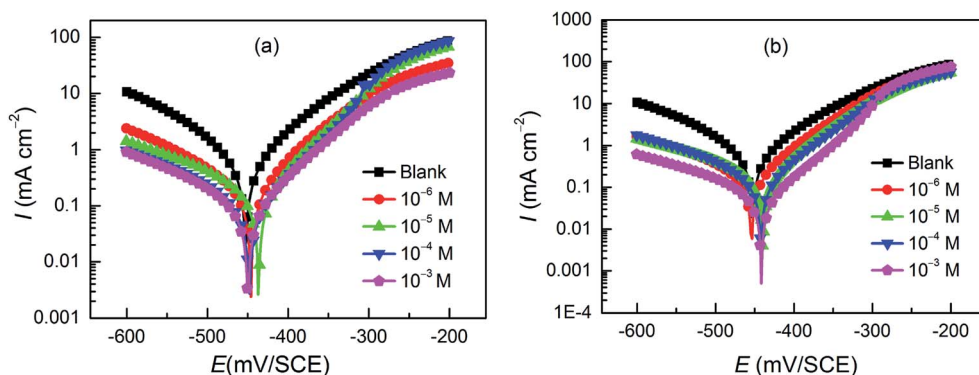
Fig. 1 Potentiodynamic polarization curves for carbon steel in the absence and presence of (a) CPT and (b) MPT at different concentrations.

interface. Considering that a double layer does not behave as an ideal capacitor in the presence of a dispersing effect, a constant phase element, CPE, is used to substitute the double layer capacitance (C_{dl}). Constant phase elements have been widely used to account for deviations brought about by surface roughness. The impedance of CPE is defined by the following equation:[30]

$$Z_{CPE} = \frac{1}{Y_0(j\omega)^n} \qquad (2)$$

where Y_0 is a proportionality coefficient, j is the imaginary unit, and ω is the angular frequency. The value of n represents the deviation from the ideal behavior and it lies between 0 and 1. C_{dl} and the inhibition efficiency IE% were calculated by the following relations:[31]

$$C_{dl} = (Y_0 R_{ct}^{1-n})^{1/n} \qquad (3)$$

$$IE(\%) = \frac{R_{ct} - R_{ct,0}}{R_{ct}} \times 100 \qquad (4)$$

where R_{ct} and $R_{ct,0}$ are the charge transfer resistance in the presence and absence of inhibitors, respectively. The corresponding impedance parameters are presented in Table 3.

It is apparent from Table 3 that the R_{ct} values of both the investigated pyrazolotriazole derivatives increase with an increase in the concentrations of the inhibitors, and MPT provides a better inhibition efficiency than CPT. However, the

values of C_{dl} decrease with an increase in the inhibitor concentration. According to the Helmholtz model, C_{dl} can be expressed as the following relation:[32]

$$C_{dl} = \frac{\varepsilon^0 \varepsilon}{d} A \qquad (5)$$

where d is the thickness of the protective film, ε is the local dielectric constant, ε^0 is the permittivity of air, and A is the effective surface area of the electrode. Then, a decrease in the CPE can result from a decrease in the local dielectric constant and/or an increase in the thickness of the double layer, suggesting that the inhibitors inhibit the corrosion of carbon steel by adsorption at the iron/acid interface. Therefore, the change in the C_{dl} values originated from the gradual displacement of the water molecules by the adsorption of the corrosion inhibitors on the iron surface, decreasing the extent of metal dissolution.[33] Overall, the corrosion inhibition performances obtained from the EIS measurements are in good agreement with those obtained from PDP.

3.3. Adsorption isotherm and thermodynamic parameters

The inhibition of the corrosion of metals by organic compounds can be explained by their adsorption isotherms. To evaluate the adsorption process of the investigated pyrazolotriazole derivatives on the carbon steel surface, several adsorption isotherms, such as Langmuir, Temkin, Freundlich and Frumkin isotherms,

Table 2 Tafel polarization parameters for carbon steel in a 1 M HCl solution in the absence of inhibitors and at different concentration of the tested inhibitors at 303 K

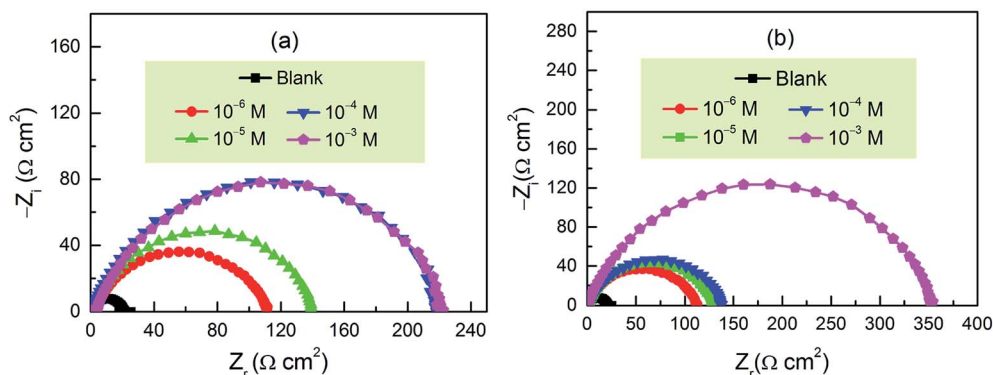| Inhibitor	C (M)	E_{corr} (mV per SCE)	I_{corr} (µA cm^{-2})	β_a (mV dec^{-1})	$-\beta_c$ (mV dec^{-1})	IE (%)
Blank	1	−452.1	660.8	95.3	113	—
CPT	10^{-6}	−445.9	128.9	64.4	99	80.4
	10^{-5}	−436.7	104.2	59.7	103.7	84.2
	10^{-4}	−447.2	72.3	69.6	104.6	89.0
	10^{-3}	−449.6	68.4	72.8	109.7	89.6
MPT	10^{-6}	−454.0	130.0	63.7	105.9	80.3
	10^{-5}	−439.3	117.8	62.4	109.8	82.1
	10^{-4}	−442.1	103.8	66.7	97.8	84.2
	10^{-3}	−441.4	42.8	67.3	99.7	93.5

Fig. 2 Nyquist plots for carbon steel in 1 M HCl in the absence and presence of (a) CPT and (b) MPT at different concentration at 303 K.
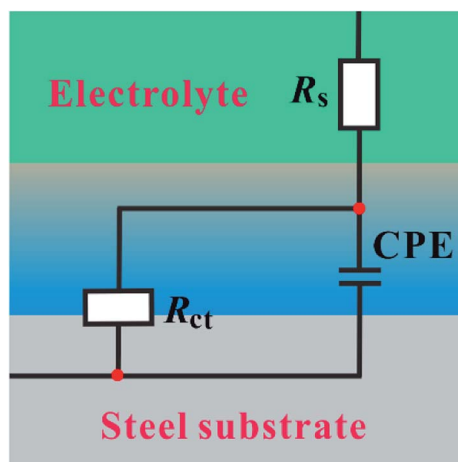

Fig. 3 Equivalent circuit used to fit the obtained Nyquist impedance spectra.

were tested. Finally, the results indicated that the Langmuir adsorption isotherm could provide the most accurate description of the adsorption behavior. The Langmuir adsorption isotherms can be expressed by the following relation:[34]

$$\frac{C}{\theta} = \frac{1}{K_{ads}} + C \qquad (6)$$

where K_{ads} is the equilibrium constant of the adsorption process, C is the corrosion inhibitor concentration in the solution, and θ is the surface coverage (from Table 3). Fig. 4 shows the plots of C/θ vs. C, which appear as straight lines for both inhibitors. The linear regression coefficients (R^2) as well as all the slopes are close to one, confirming that the adsorption of pyrazolotriazole follows the Langmuir adsorption isotherm. The free energy of adsorption ΔG^0_{ads} can be calculated from the K_{ads} value by the following correlation:[35]

$$\Delta G^0_{ads} = -RT \ln(K_{ads} \times 55.5) \qquad (7)$$

where 55.5 is the concentration of water, R is the universal gas constant and T is the absolute temperature. As can be observed from Fig. 4, the calculated ΔG^0_{ads} values for CPT and MPT are -37.5 and -31.2 kJ mol^{-1}, respectively. These negative values suggested that the adsorption of both compounds on the carbon steel surface was a spontaneous process. It is generally accepted that the ΔG^0_{ads} values of -20 kJ mol^{-1} or less negative than this are associated with an electrostatic interaction between the charged molecules and the charged metal surface (physical adsorption), whereas those of -40 kJ mol^{-1} or more negative than this involve charge sharing or transfer between the inhibitor molecules and metals (chemical adsorption).[36] However, the adsorption of inhibitors on the metal substrates cannot be

Table 3 EIS parameters obtained for carbon steel in a 1 M HCl solution in the absence of inhibitors and at different concentrations of the tested inhibitors at 303 K

|	C (M)	R_s (Ω cm^2)	R_{ct} (Ω cm^2)	CPE Y_0 ($\times 10^{-4}$ Ω^{-1} cm^{-2} s^n)	n	C_{dl} (μF cm^{-2})	IE (%)	θ
Blank		0.568	20.24	2.72	0.860	116.87	—	—
CPT	10^{-6}	2.933	107.5	1.67	0.774	51.87	81.1	0.811
	10^{-5}	1.589	139.5	1.38	0.777	44.50	85.4	0.854
	10^{-4}	1.145	218.0	1.02	0.806	40.09	90.7	0.907
	10^{-3}	2.685	219.7	1.01	0.795	37.98	90.8	0.908
MPT	10^{-6}	1.324	109.3	1.48	0.798	52.17	81.4	0.814
	10^{-5}	1.870	125.1	1.35	0.803	49.82	83.8	0.838
	10^{-4}	1.273	135.9	1.27	0.780	40.47	85.1	0.851
	10^{-3}	1.119	351.9	0.89	0.794	36.62	94.2	0.942
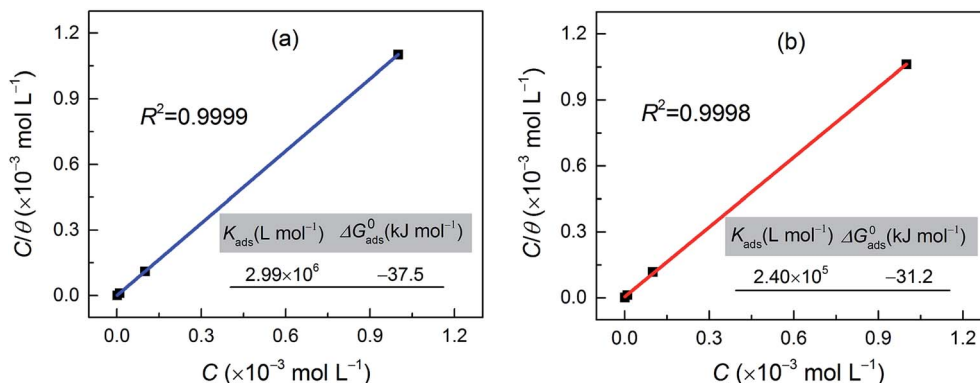
Fig. 4 Langmuir adsorption isotherms and relevant parameters for the investigated (a) CPT and (b) MPT inhibitors on the carbon steel surface at 303 K.

considered as a purely physical or chemical behaviour. In addition to chemical adsorption, the inhibitor molecules can also be adsorbed on the metal surface *via* physical interactions. In this case, we can conclude that the adsorption of pyrazolotriazoles on iron substrates is a mixed type of chemical and physical adsorption, with the first process being predominant.

3.4. Effect of temperature

As shown in Fig. 5, the effect of temperature on the corrosion of carbon steel in 1 M HCl without and with the studied inhibitors at various concentrations was investigated between 303 K and 333 K using the PDP measurements. The deduced corrosion parameters such as E_{corr}, I_{corr}, and the inhibition efficiency (IE%) are summarized in Table 4. It is clear that the corrosion rate increases with an increase in temperature under all circumstances. The corrosion rate of carbon steel in the absence of inhibitors increased steeply from 303 to 333 K, whereas the corrosion rate increased slowly in the presence of inhibitors. The inhibition efficiency decreased with an increase in temperature from 303 to 333 K. This type of behavior can be described on the basis that the increase in temperature leads to a shift in the equilibrium position of the adsorption/desorption
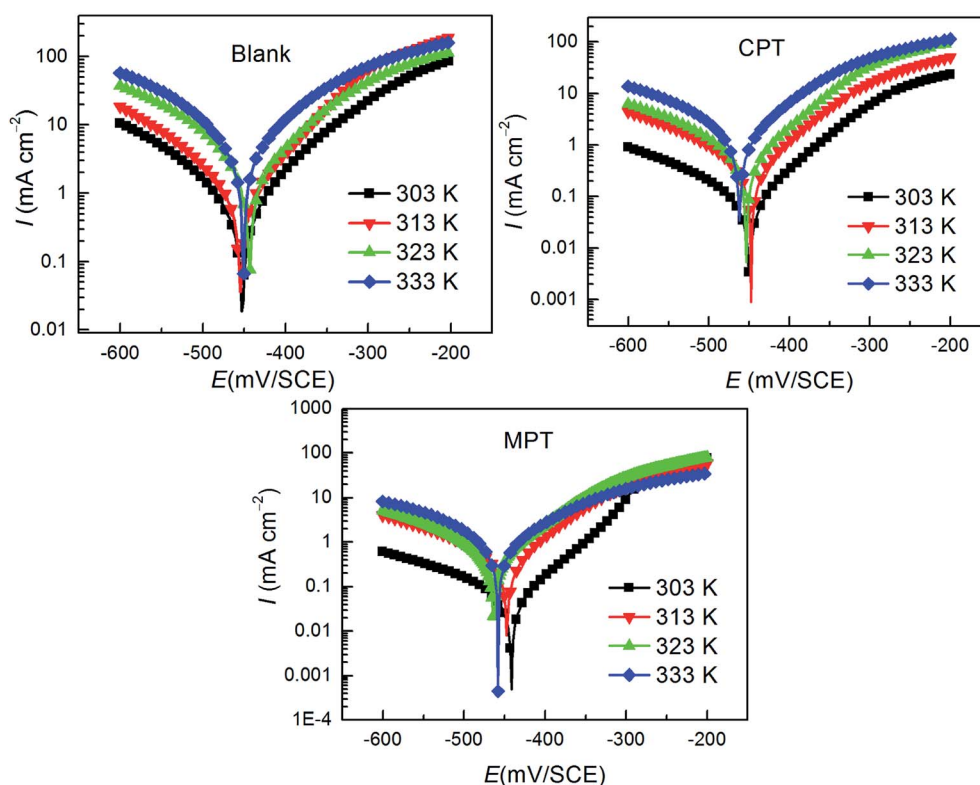

Fig. 5 Effect of temperature on the behavior of the carbon steel/HCl interface in uninhibited and inhibited solutions with 10^{-3} M of the inhibitors tested herein.

Table 4 The influence of temperature on the PDP parameters for carbon steel in 1 M HCl with and without the studied inhibitors in the temperature range of 303–333 K

Inhibitor	T (K)	E_{corr} (mV per SCE)	I_{corr} (μA cm^{-2})	β_a (mV dec^{-1})	$-\beta_c$ (mV dec^{-1})	IE (%)	θ
Blank	303	−452.1	660.8	95.3	113	—	—
	313	−454.4	865.5	79.1	95.4	—	—
	323	−443.4	1529.8	88.7	79.3	—	—
	333	−450.8	2898.3	82.8	82.9	—	—
CPT	303	−449.6	68.4	72.8	109.7	89.6	0.896
	313	−447.4	253.7	71.6	94.6	70.6	0.706
	323	−453.0	506.8	79.8	114.8	66.8	0.668
	333	−461.2	1360.8	88.9	117.7	53.0	0.530
MPT	303	−441.4	42.8	67.3	99.7	93.5	0.935
	313	−447.0	264.4	67.9	99.4	69.4	0.694
	323	−463.1	485.8	85.5	117.2	68.2	0.682
	333	−457.9	928.6	116.7	128.4	67.9	0.679

phenomenon towards the desorption of the inhibitor molecules on the surface of the carbon steel.[37]

The effect of temperature on the corrosion current (I_{corr}) can be used to determine the activation thermodynamic parameters for the dissolution process following the Arrhenius and transition-state equations:[38]

$$\ln I_{corr} = \ln A - \frac{E_a}{RT} \tag{8}$$

$$\ln \frac{I_{corr}}{T} = \ln \frac{R}{Nh} + \frac{\Delta S_a}{R} - \frac{\Delta H_a}{RT} \tag{9}$$

where E_a is the activation corrosion energy, ΔH_a is the enthalpy, ΔS_a is the entropy of activation, T is the absolute temperature in Kelvin, h is the Planck's constant, N is Avogadro's number and R is the molar gas constant. The plots of $\ln I_{corr}$ vs. $1/T$ and $\ln(I_{corr}/T)$ vs. $1/T$ are shown in Fig. 6. The E_a values for carbon steel were determined from the slope of the $\ln I_{corr}$ vs. $1/T$ plots. ΔH_a and ΔS_a were calculated from the slope and intercept of the $\ln(I_{corr}/T)$ vs. $1/T$ plots, respectively. The obtained corrosion kinetic parameters are listed in Table 5.

As can be observed from Table 5, the values of E_a for the inhibitor-containing systems are higher than that for the uninhibited system; this indicates a decrease in the rate of

dissolution of carbon steel due to an increase in the energy barrier for the dissolution reaction. The positive sign of ΔH_a suggests that the dissolution of carbon steel is endothermic.[39] The large negative value of ΔS_a for carbon steel in 1 M HCl implies that the formation of the activated complex is the rate-determining step, rather than the dissociation step. In the presence of the inhibitors studied herein, the ΔS_a value increased, indicating an increase in disorder as the reactants were converted to the activated complexes.[40]

3.5. DFT results

The DFT study was conducted to understand and explain the inhibitory effects of compounds in molecular terms. The HOMO and LUMO orbitals are useful for predicting adsorption centers in the interaction between the inhibitor and the metal surface. Efficient inhibitors donate electrons (a nucleophilic attack) to the d orbital of the metal and accept electrons from the metal surface (an electrophilic attack).[41] The frontier molecular orbitals for the synthesized inhibitors in both the neutral and the protonated forms are displayed in Fig. 7. The HOMO orbitals are delocalized over the pyrazolotriazole moiety for CPT, whereas for MPT, the HOMO orbitals are mainly localized over the carbothioamide moiety. On the other hand,
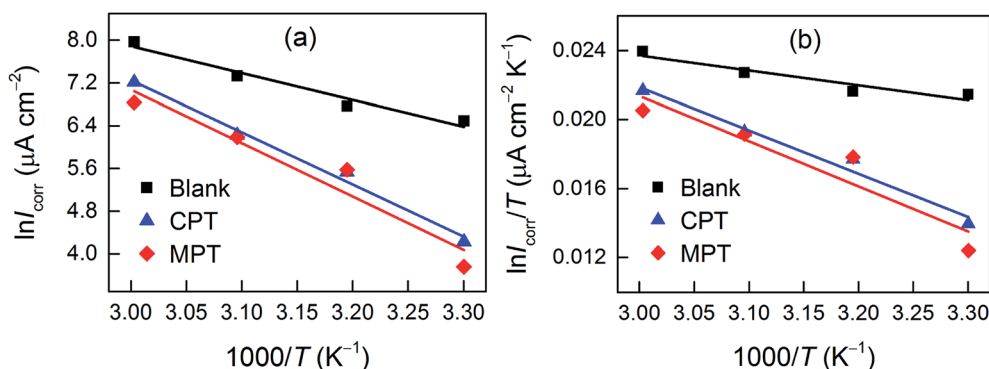
Fig. 6 (a) Arrhenius plots of $\ln I_{corr}$ vs. $1/T$ and transition-state plots of $\ln(I_{corr}/T)$ vs. $1/T$ (b) for carbon steel in 1 M HCl containing 10^{-3} M CPT and MPT at various temperatures.

Table 5 Corrosion kinetic parameters for carbon steel in 1 M HCl in the absence and presence of 10^{-3} M of tested inhibitors

Inhibitor	E_a (kJ mol^{-1})	ΔH_a (kJ mol^{-1})	ΔS_a (J mol^{-1} K^{-1})
Blank	41.7	39.1	−62.8
CPT	81.1	80.5	56.3
MPT	83.4	76.1	40.2

the LUMO orbital of CPT is delocalized over the triazole ring, similar to the case of the carbothioamide group for MPT. The electronic density delocalization of the HOMO and LUMO orbitals distinctly showed that the synthesized inhibitors might donate/accept the electrons of the atom sites in the triazol and pyrazolo moieties to/from the d-orbitals of the iron metal. This phenomenon is more pronounced for protonated inhibitors.

Using the Koopmans' theorem as an approximation,[42] the ionization potential (I) and electron affinity (A) can be replaced by the highest occupied molecular orbital energy (E_{HOMO}) and the lowest unoccupied molecular orbital energy (E_{LUMO}), respectively. That is, $I = -E_{HOMO}$ and $A = -E_{LUMO}$. The electronegativity (χ) and global hardness (η) are related to I and A:[43]

$$\chi = \frac{I + A}{2} \tag{10}$$

$$\eta = \frac{I - A}{2} \tag{11}$$

The fraction of electrons transferred from (to) the inhibitor molecules to (from) the metallic surface (ΔN) was calculated by[44]

$$\Delta N = \frac{\chi_{Fe} - \chi_{inh}}{2(\eta_{Fe} + \eta_{inh})} = \frac{\Phi_{Fe} - \chi_{inh}}{2\eta_{inh}} \tag{12}$$

For the iron surface, the work-function Φ is taken as its electronegativity, whereas the chemical hardness is neglected because η of the bulk metals is related to the inverse of their density of states at the Fermi level, which is an exceedingly small number.[45] The relative quantum chemical descriptors are listed in Table 6. From the data, we can observe that MPT exhibits lower ΔE value and higher ΔN and dipole moment (μ) values, which theoretically confirm that it has a better corrosion inhibition performance.

3.6. Molecular dynamics simulation

MD simulations were carried out to provide deep insights into the anticorrosive mechanism of the studied inhibitors, which helped us to better understand the inhibitor–iron interactions at the atomic and molecular level. The simulations were run until the system reached equilibrium and both the energy and temperature were balanced. The equilibrium configurations of CPT and MPT adsorbed on the Fe(110) surface are presented in Fig. 8. Moreover, we declare that the absorption behavior of the inhibitors in the protonated form has no obvious effect on their equilibrium configurations (see Fig. S5 in the ESI†); therefore, we have concentrated on the neutral results in the following discussions.

As shown in Fig. 8a and b, the inhibitor molecules were adsorbed on the Fe(110) surface in the parallel adsorption mode. Hence, it was reasonable that the nearly flat adsorption orientation was ascribed to the simultaneous interactions of the inhibitor molecules with the Fe(110) surface through the electron-rich groups as well as the aromatic rings. Compared with the case of vertical adsorption, the parallel adsorption configurations can distinctly cover more steel surface area and this leads to a better inhibition action.[46]

The strength of the corrosion inhibitors absorbed on the iron surface can be expressed by the adsorption energy (E_{ads}), which has been calculated using the following equation:[47]
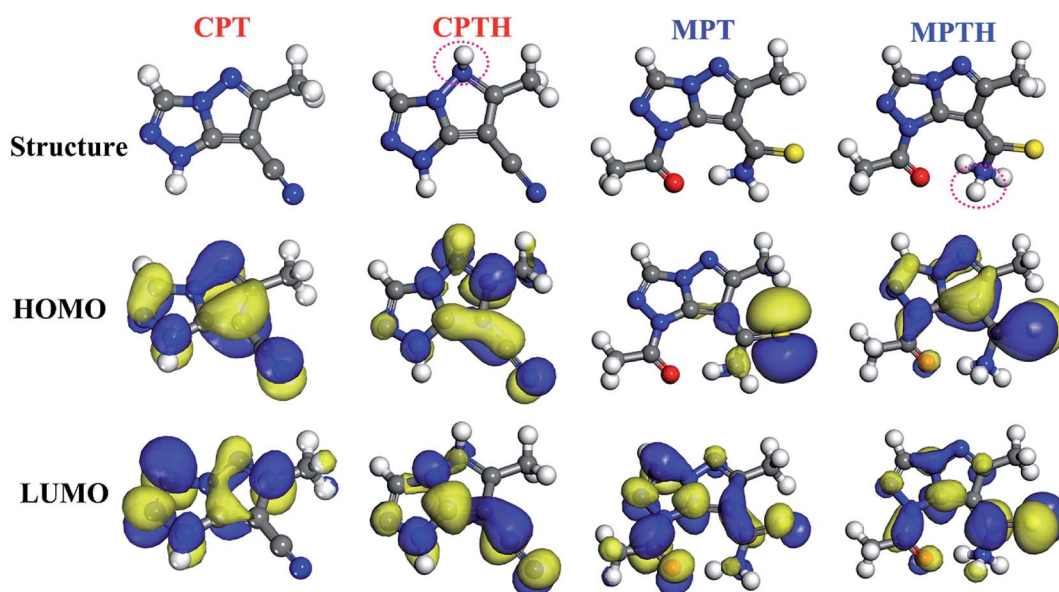
Fig. 7 Frontier molecular orbitals of the synthesized inhibitors in the neutral and protonated forms.

Table 6 Some molecular properties of the tilted compounds calculated using DFT at the B3LYP level in an aqueous phase

Inhibitor	I (eV)	A (eV)	E_{HOMO} (eV)	E_{LUMO} (eV)	ΔE (eV)	χ	η	ΔN	μ (Debye)
CPT	6.66	0.85	−6.66	−0.85	5.81	3.75	2.91	0.558	4.11
CPTH	7.85	2.11	−7.85	−2.11	5.74	4.98	2.87	0.351	7.64
MPT	6.26	1.92	−6.26	−1.92	4.34	4.09	2.17	0.671	5.51
MPTH	7.20	3.41	−7.20	−3.41	3.79	5.30	1.89	0.449	9.31

$$E_{ads} = E_{total} - (E_{surf+water} + E_{inh+water}) + E_{water} \tag{13}$$

where E_{total} is the total potential energy of the system, which includes the iron crystal, the adsorbed inhibitor molecule and the solution. $E_{surf+water}$ and $E_{inh+water}$ are the potential energies of the system without the inhibitor and the system without the iron crystal, respectively. E_{water} is the potential energy of the water molecules.

The adsorption energies in the present study were calculated from the average adsorption energy of the obtained equilibrium configurations. The obtained E_{ads} values are −335.2, −512.7, −348.9, and −523.4 kJ mol^{-1} for CPT, MPT, CPTH, and MPTH, respectively. The negative values indicate that spontaneous adsorption can be expected. It is generally accepted that a more negative value of E_{ads} suggests a stronger adsorption strength between the inhibitor molecule and the metal substrate.[48] Obviously, MPT has a better inhibition performance with a higher absolute value of E_{ads}.

Finally, pair correlation functions for the super-molecular structures, $g(r)$, were obtained. Generally, the peak in the $g(r)$–

r curve within 0.35 nm was caused by chemical bonds, and the peak outside 0.35 nm was caused by the Coulomb and van der Waals interactions.[49] As shown in Fig. 8c and d, the distance between CPT/MPT and the iron atoms of the Fe(110) face was 0.307/0.335 nm, less than 0.350 nm, which indicated that chemical bonds had formed between these two compounds and the iron atoms. Moreover, the countless decentralized peaks located outside 0.35 nm, which were derived from physical interactions, might also contribute to the net molecule surface attraction.

3.7. Mechanism of adsorption and inhibition

As illustrated in Fig. 9, a mechanism was proposed to explain the high corrosion inhibition performance of the studied inhibitors (abbreviated as Inh). The cathodic chemical process may occur as follows:[50]

$$Fe + H^+ \rightarrow (FeH^+)_{ads} \tag{14}$$

$$(FeH^+)_{ads} + e^- \rightarrow (FeH)_{ads} \tag{15}$$
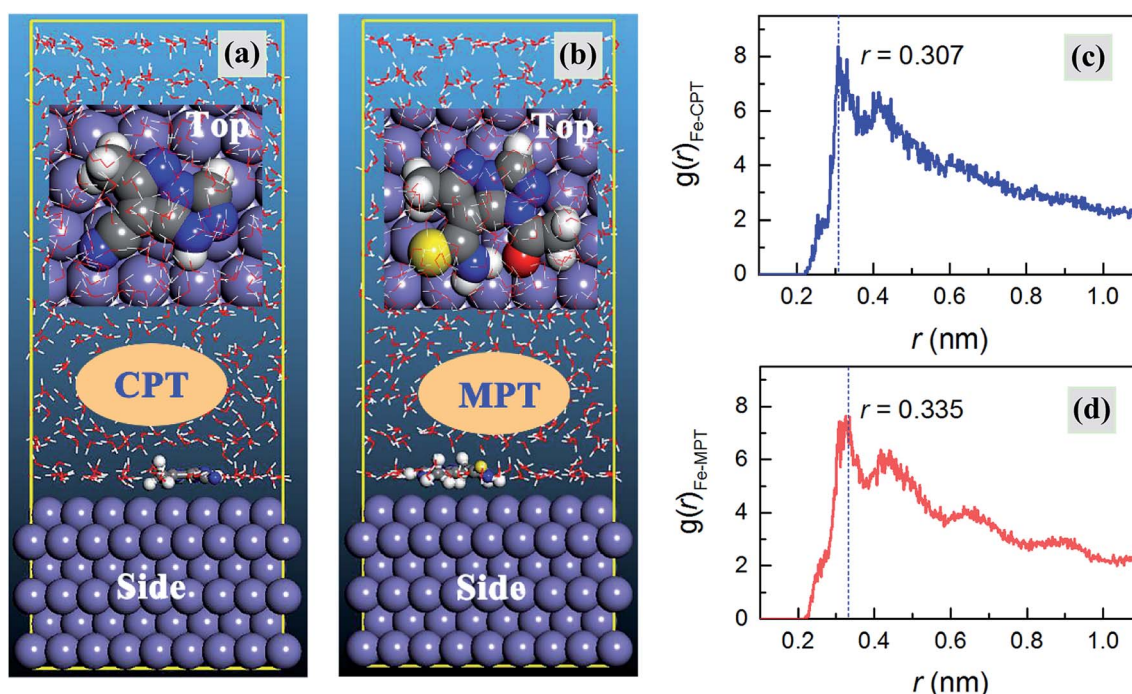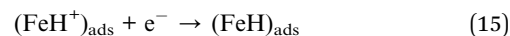
Fig. 8 (a and b) Equilibrium configurations and (c and d) radial distribution functions for the CPT and MPT molecules on an Fe(110) surface in the aqueous phase, respectively.
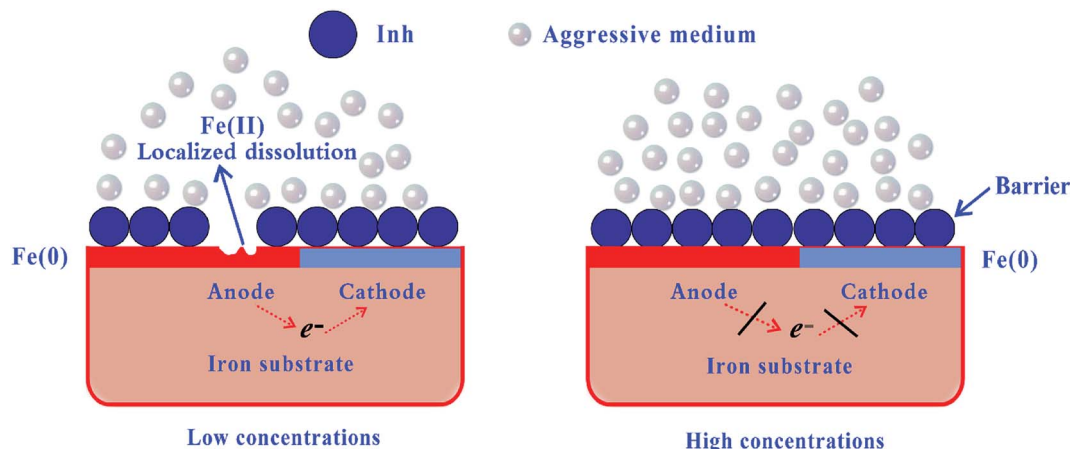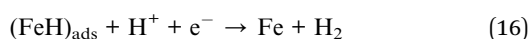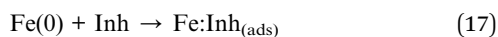
Fig. 9 Proposed mechanism for the adsorption of inhibitor molecules on the iron surface in an aggressive medium.

$$(\text{FeH})_{\text{ads}} + H^+ + e^- \rightarrow Fe + H_2 \qquad (16)$$

The corrosion inhibition can be attributed to the formation of an adsorbed layer of corrosion inhibitor molecules, *i.e.*

$$Fe(0) + Inh \rightarrow Fe{:}Inh_{\text{(ads)}} \qquad (17)$$

where $Fe{:}Inh_{\text{(ads)}}$ refers to inhibitor molecules adsorbed on the iron surface. We can find that at low inhibitor concentrations, localized corrosion can occur in the anode area, where the corresponding reaction is the dissolution of metallic iron (Fe^0) to ferrous cations (Fe^{2+}). However, a perfect organic film can be formed on the iron surface at high inhibitor concentrations, which can be regarded as a barrier to iron dissolution and hydrogen reduction. Several types of adsorption may take place in the inhibition phenomena involving the adsorption of the CPT/MPT molecules on the iron surface as follows: (i) a non-covalent interaction of the CPT/MPT (or protonated) molecules with iron atoms (physisorption); (ii) an interaction between the unshared electron pairs of the N/O/S atoms or the π-electrons of aromatic rings and the iron surface (chemisorption); and (iii) a combination of the abovementioned processes.

4. Conclusions

The abovementioned results show the excellent performance of the pyrazolotriazole derivatives MPT and CPT for the inhibition of carbon steel corrosion in 1 M HCl. The higher efficiency of MPT when compared with that of CPT was due to the presence of a sulfur atom in MPT. The inhibition efficiency increased with the increasing inhibitor concentration. The quantum chemical calculation results revealed that the electron-rich groups as well as the aromatic rings were active sites *via* which the inhibitors adsorbed onto the carbon steel surface by sharing electrons with iron atoms. The molecular dynamics simulation results revealed that both inhibitors adsorbed on the iron surface in a nearby flat manner.

Conflicts of interest

There are no conflicts to declare.

Acknowledgements

References

1 X. G. Li, D. W. Zhang, Z. Y. Liu, Z. Li, C. W. Du and C. F. Dong, *Nature*, 2015, **527**, 441–442.
2 D. Dwivedi, K. Lepková and T. Becker, *RSC Adv.*, 2017, **7**, 4580–4610.
3 B. Tan, S. Zhang, H. Liu, Y. Qiang, W. Li, L. Guo and S. Chen, *J. Taiwan Inst. Chem. Eng.*, 2019, **102**, 424–437.
4 A. A. Al-Amiery, A. A. H. Kadhum, A. H. M. Alobaidy, A. B. Mohamad and P. S. Hoon, *Materials*, 2014, **7**, 662–672.
5 Y. G. Avdeev and Y. I. Kuznetsov, *Russ. Chem. Rev.*, 2012, **81**, 1133–1145.
6 M. Finšgar and J. Jackson, *Corros. Sci.*, 2014, **86**, 17–41.
7 S. Marzorati, L. Verotta and S. P. Trasatti, *Molecules*, 2019, **24**, 48.
8 M. Goyal, S. Kumar, I. Bahadur, C. Verma and E. E. Ebenso, *J. Mol. Liq.*, 2018, **256**, 565–573.
9 L. Guo, I. B. Obot, X. Zheng, X. Shen, Y. Qiang, S. Kaya and C. Kaya, *Appl. Surf. Sci.*, 2017, **406**, 301–306.
10 F. Himo, *Theor. Chem. Acc.*, 2005, **116**, 232–240.
11 I. B. Obot and Z. M. Gasem, *Corros. Sci.*, 2014, **83**, 359–366.
12 A. A. Al-Sarawya, A. S. Fouda and W. A. S. El-Dein, *Desalination*, 2008, **229**, 279–293.

13 N. O. Obi-Egbedi, I. B. Obot, M. I. El-Khaiary, S. A. Umoren and E. E. Ebenso, *Int. J. Electrochem. Sci.*, 2011, **6**, 5649–5675.

14 D. A. Winkler, M. Breedon, A. E. Hughes, F. R. Burden, A. S. Barnard, T. G. Harvey and I. Cole, *Green Chem.*, 2014, **16**, 3349–3357.

15 M. Gholami, I. Danaee, M. H. Maddahy and M. RashvandAvei, *Ind. Eng. Chem. Res.*, 2013, **52**, 14875–14889.

16 K. F. Khaled, *Electrochim. Acta*, 2008, **53**, 3484–3492.

17 Y. S. Li, H. Tian, D. S. Zhao, D. K. Hu, X. Y. Liu, H. W. Jin, G. P. Song and Z. N. Cui, *Bioorg. Med. Chem. Lett.*, 2016, **26**, 3632–3635.

18 J. Nalawade, A. Shinde, A. Chavan, S. Patil, M. Suryavanshi, M. Modak, P. Choudhari, V. D. Bobade and P. C. Mhaske, *Eur. J. Med. Chem.*, 2019, **179**, 649–659.

19 W. H. Li, Q. He, S. T. Zhang, C. L. Pei and B. R. Hou, *J. Appl. Electrochem.*, 2008, **38**, 289–295.

20 C. M. Fernandes, L. X. Alvarez, N. E. dos Santos, A. C. M. Barrios and E. A. Ponzio, *Corros. Sci.*, 2019, **149**, 185–194.

21 S. Kaya, P. Banerjee, S. K. Saha, B. Tüzün and C. Kaya, *RSC Adv.*, 2016, **6**, 74550–74559.

22 R. D. Snyder, G. S. Pearl, G. Mandakas, W. N. Choy, F. Goodsaid and I. Y. Rosenblum, *Environ. Mol. Mutagen.*, 2004, **43**, 143–158.

23 M. P. Andersson and P. Uvdal, *J. Phys. Chem. A*, 2005, **109**, 2937–2941.

24 E. Cances, B. Mennucci and J. Tomasi, *J. Chem. Phys.*, 1997, **107**, 3032–3041.

25 L. Guo, S. Zhu, S. Zhang, Q. He and W. Li, *Corros. Sci.*, 2014, **87**, 366–375.

26 H. Sun, *J. Phys. Chem. B*, 1998, **102**, 7338–7364.

27 M. Yadav, S. Kumar and L. Gope, *J. Adhes. Sci. Technol.*, 2014, **28**, 1072–1089.

28 Z. Salarvand, M. Amirnasr, M. Talebian, K. Raeissi and S. Meghdadi, *Corros. Sci.*, 2017, **114**, 133–145.

29 E. E. Elemike, H. U. Nwankwo and D. C. Onwudiwe, *J. Mol. Struct.*, 2018, **1155**, 123–132.

30 K. F. Khaled and N. Hackerman, *Mater. Chem. Phys.*, 2003, **82**, 949–960.

31 T. M. Lv, S. H. Zhu, L. Guo and S. T. Zhang, *Res. Chem. Intermed.*, 2015, **41**, 7073–7093.

32 N. Muhammad, Y. A. Elsheikh, M. I. A. Mutalib, A. A. Bazmi, R. A. Khan, H. Khan, S. Rafiq, Z. Man and I. Khan, *J. Ind. Eng. Chem.*, 2015, **21**, 1–10.

33 L. Guo, S. T. Zhang, W. P. Li, G. Hu and X. Li, *Mater. Corros.*, 2014, **65**, 935–942.

34 H. Gerengi, H. I. Ugras, M. M. Solomon, S. A. Umoren, M. Kurtay and N. Atar, *J. Adhes. Sci. Technol.*, 2016, **30**, 2383–2403.

35 N. Esmaeili, J. Neshati and I. Yavari, *Res. Chem. Intermed.*, 2016, **42**, 5339–5351.

36 R. Solmaz, *Corros. Sci.*, 2014, **79**, 169–176.

37 M. M. Solomon, S. A. Umoren, I. B. Obot, A. A. Sorour and H. Gerengi, *ACS Appl. Mater. Interfaces*, 2018, **10**, 28112–28129.

38 M. A. Deyab and S. S. Abd El-Rehimb, *J. Taiwan Inst. Chem. Eng.*, 2014, **45**, 1065–1072.

39 R. Karthikaiselvi, S. Subhashini and R. Rajalakshmi, *Arabian J. Chem.*, 2012, **5**, 517–522.

40 A. Zarrouk, B. Hammouti, A. Dafali and F. Bentiss, *Ind. Eng. Chem. Res.*, 2013, **52**, 2560–2568.

41 I. B. Obot, D. D. Macdonald and Z. M. Gasem, *Corros. Sci.*, 2015, **99**, 1–30.

42 R. C. Morrison, *J. Chem. Phys.*, 1992, **96**, 3718–3722.

43 S. B. Liu, *Acta Phys.-Chim. Sin.*, 2009, **25**, 590–600.

44 L. H. Madkour, S. Kaya and I. B. Obot, *J. Mol. Liq.*, 2018, **260**, 351–374.

45 A. Kokalj, *Electrochim. Acta*, 2010, **56**, 745–755.

46 X. Li, S. Deng, T. Lin, X. Xie and G. Du, *Corros. Sci.*, 2017, **118**, 202–216.

47 Y. Gong, Z. Wang, F. Gao, S. Zhang and H. Li, *Ind. Eng. Chem. Res.*, 2015, **54**, 12242–12253.

48 Y. El Bakri, L. Guo, E. H. Anouar, A. Harmaoui, A. Ben Ali, E. M. Essassi and J. T. Mague, *J. Mol. Struct.*, 2019, **1176**, 290–297.

49 J. P. Zeng, J. Y. Zhang and X. D. Gong, *Comput. Theor. Chem.*, 2011, **963**, 110–114.

50 A. Doner, R. Solmaz, M. Ozcan and G. Kardas, *Corros. Sci.*, 2011, **53**, 2902–2913.